Hindawi
Advances in Condensed Matter Physics
Volume 2018, Article ID 1217639, 7 pages
https://doi.org/10.1155/2018/1217639

Research Article

Improved Electrochemical Performance of $Li_{1.25}Ni_{0.2}Co_{0.333}Fe_{0.133}Mn_{0.333}O_2$ Cathode Material Synthesized by the Polyvinyl Alcohol Auxiliary Sol-Gel Process for Lithium-Ion Batteries

He Wang, Mingning Chang, Yonglei Zheng, Ningning Li, Siheng Chen, Yong Wan, Feng Yuan, Weiquan Shao, and Sheng Xu

College of Physics, Qingdao University, Qingdao 266071, China

Correspondence should be addressed to Sheng Xu; shengxu@qdu.edu.cn

Received 26 October 2018; Revised 17 November 2018; Accepted 22 November 2018; Published 10 December 2018

Guest Editor: Hong Fang

Copyright © 2018 He Wang et al. This is an open access article distributed under the Creative Commons Attribution License, which permits unrestricted use, distribution, and reproduction in any medium, provided the original work is properly cited.

A lithium-rich manganese-based cathode material, $Li_{1.25}Ni_{0.2}Co_{0.333}Fe_{0.133}Mn_{0.333}O_2$, was prepared using a polyvinyl alcohol (PVA)-auxiliary sol-gel process using MnO_2 as a template. The effect of the PVA content (0.0–15.0 wt%) on the electrochemical properties and morphology of $Li_{1.25}Ni_{0.2}Co_{0.333}Fe_{0.133}Mn_{0.333}O_2$ was investigated. Analysis of $Li_{1.25}Ni_{0.2}Co_{0.333}Fe_{0.133}Mn_{0.333}O_2$ X-ray diffraction patterns by RIETAN-FP program confirmed the layered α-$NaFeO_2$ structure. The discharge capacity and coulombic efficiency of $Li_{1.25}Ni_{0.2}Co_{0.333}Fe_{0.133}Mn_{0.333}O_2$ in the first cycle were improved with increasing PVA content. In particular, the best material reached a first discharge capacity of 206.0 $mAhg^{-1}$ and best rate capability (74.8 $mAhg^{-1}$ at 5 C). Meanwhile, the highest capacity retention was 87.7% for 50 cycles. Finally, electrochemical impedance spectroscopy shows that as the PVA content increases, the charge-transfer resistance decreases.

1. Introduction

Rapid development of lithium-ion battery technology and the environmental impact of traditional non-renewable energy sources are driving considerable interest in efficient "green" energy storage devices [1]. Currently, the energy storage devices of new energy vehicles and various electronic devices (laptops, cell phones, power tools, bluetooth devices, etc.) usually use lithium ion secondary batteries (LIBs). $LiCoO_2$ was the first cathode material used for commercial LIBs because of its high operating voltage and ease of preparation [2, 3]. But, the high cost, and toxicity of layered $LiCoO_2$ limit its use for large-scale high-power applications. Replaceable cathode materials, $Li_{1.2}Ni_{0.2}Mn_{0.6}O_2$, $LiMn_2O_4$, $LiFePO_4$, $LiNi_{1/3}Co_{1/3}Mn_{1/3}O_2$, and $LiNi_{0.8}Co_{0.15}Mn_{0.05}O_2$, have previously been synthesized [4–8]. Despite its unsatisfactory capacity (120–140 $mAhg^{-1}$), the layered-structure $LiNi_xCo_yMn_{1-x-y}O_2$ is considered a promising cathode material because of its relatively low cost and reduced toxicity [9, 10]. To address the capacity issue, researchers have launched a series of explorations to identify high-capacity lithium storage cathode materials.

The specific capacity and stability of LIBs can be effectively improved by doping or changing the surface morphology or through surface modification. Mohan et al. synthesized $LiFe_xNi_{1-x}O_2$ ($0.00 \leq x \leq 0.20$) nanoparticles with a single-layer structure using a sol-gel approach. The particle size was reduced with the substitution of iron, thereby improving the electrochemical properties of the cathode material [11]. The surface-modified layer of the cathode improves the cycle efficiency and thermal stability for high-rate discharge and improves the conductivity of the material surface [12–14].

In this work, we used the well-known sol-gel process to synthesize the target material $Li_{1.25}Ni_{0.2}Co_{0.333}Fe_{0.133}Mn_{0.333}O_2$ by controlling the PVA content (0.0–15.0 wt%). Scanning electron microscopy (SEM), electrochemical tests, and X-ray diffraction (XRD)

were used to investigate the relationship between the PVA doping ratio and specific capacity of the synthesized cathode materials. Pretreatment can significantly improve the rate performance and initial coulomb efficiency and also help to improve cycle stability and suppress voltage attenuation. These properties are expected to improve the capacity utilization and rate capability of this material [15].

2. Experimental Section

2.1. Material Synthesis. Using a method previously reported in the literature, $MnCO_3$ microspheres were prepared. First, 1.183 g $MnSO_4$ was dissolved in a mixture of ultrapure water (conductivity of 0.05 μScm^{-1}) and alcohol labeled "A." Then, 5.53 g NH_4HCO_3 was dissolved in 490 ml of ultrapure water without alcohol labeled "B." When both A and B are fully dissolved, the two solutions A and B are mixed together to form a suspension. The suspension was stirred constantly at room temperature for 5 h. Then, the white precipitate in the suspension was separated by centrifugation; the precipitate was identified as $MnCO_3$. Next, the $MnCO_3$ was washed with a mixed solution of alcohol and ultrapure water. After cleaning, place $MnCO_3$ on a drying table and dry it in a 60°C air atmosphere for 6 h.

Second, MnO_2 hollow microspheres were prepared by mixing the precursor $MnCO_3$ and an aqueous 0.033 M $KMnO_4$ solution. After removing the $MnCO_3$ core with 0.03 M HCl, MnO_2 hollow microspheres were obtained after centrifugation. The microspheres were cleaned 3 times with ultrapure water. Next, MnO_2 was dried using a drying oven under an air atmosphere.

Finally, $Li_{1.25}Ni_{0.2}Co_{0.333}Fe_{0.133}Mn_{0.333}O_2$ was prepared using the following PVA-auxiliary sol-gel process. Weigh a certain amount of $LiOH{\cdot}H_2O$, $Fe(NO_3)_3{\cdot}9H_2O$, $Ni(NO_3)_2{\cdot}6H_2O$, $Co(NO_3)_2{\cdot}6H_2O$, the MnO_2 microspheres were dissolved in 60 ml of ultrapure water, and the lithium/metal (Ni, Mn, Fe) molar ratio is 1.25. Since lithium is depleted under high temperature conditions, it is necessary to add an excessive amount of lithium. In order to ensure sufficient reaction of raw materials, PVA and citric acid were added successively in different time. The mass fractions of PVA were x = 0.0, 2.5, 5.0, 7.5, 9.0, 10.0, 11.0, 12.5, and 15.0 wt%. The molar ratio of citric acid to total metal ions was 1:1 [16]. The mixture was then stirred at 80°C until a viscous gel was obtained [17]. The treatment of the precursor was divided into two steps, first drying at 120°C for 12 h and then heating to 450°C for 6 h in air.

The final products were obtained by finely grinding the gel followed by heat treatment at 950°C under a non-rare gas atmosphere for 12 h.

3. Results and Discussion

3.1. Sample Characterization. We first investigated the structural features of the MnO_2 hollow microsphere samples and PVA-auxiliary lithium-rich manganese-based cathode samples using SEM. The spherical shell structure and broken hollow microspheres of the MnO_2 are shown in Figures 1(a) and 1(b), respectively. Both of their diameters were approximately 1 – 2 μm. All of the samples exhibited a shell structure that was gradually destroyed with increasing x while the layered structure was aggregated together, which greatly increased the contact surface area in the scanned area. The tendency toward aggregation decreased with increasing x in Figures 1(c)–1(i). For x = 10.0 wt%, the sample has the smallest particle size and the most uniform distribution. It is well known that electrochemical lithium insertion/extraction is much easier in small particles, because of the reduction of diffusion pathways for Li^+ ions, which also enables faster electronic transport through the size effect [19].

4. Characterization

The X-ray diffraction (Rigaku SmArtlab-3KW) patterns were collected on a D8 Advance instrument with Cu Kα radiation operated at 40 KV, 40 mA and scanning step 2 degrees per minute at room temperature from 10° to 80°. The XRD results were analyzed using the RIETAN-FP program. SEM (JEOL JSM-6390) was usually applied to analyze the morphology of the resulting materials.

Electrochemical Measurements. The electrochemical measurements of terrestrial CR2025 batteries were performed at room temperature using CR2025 coin cells. The active substances, acetylene black and poly (vinylidene fluoride) were dissolved in N-methyl-2-pyrrolidone (NMP) at a ratio of 8:1:1, and then the cathode compounds were evenly coated on the aluminium foil by a smearing machine. Firstly, the smear was dried in 50°C air for 6 hours, and then dried in 120°C vacuum for 12 hours. The coin cells were assembled in a glove box (H_2O < 1ppm, O_2 < 1ppm) using Li metal foil as the counter electrodes and 1 M $LiPF_6$ in a 1:1 v/v mixture of ethylene carbonate and diethyl carbonate as the electrolyte. The assembled battery was subjected to a charge and discharge cycle test at different magnifications, and the voltage range was controlled within 2.5 to 4.5 V. The electrochemical impedance spectroscopy spectra were obtained in the frequency range of 10^{-1} Hz to 10^5 Hz using a PARSTAT 2273 electrochemical work station [18].

Figure 2 presents a prototypical example of the XRD powder pattern of $Li_{1.25}Ni_{0.2}Co_{0.333}Fe_{0.133}Mn_{0.333}O_2$ (x = 10.0 wt%). The pattern was obtained using the RIETAN-FP program. The powder pattern reproduces well the typical features of the α-$NaFeO_2$ structure and can be indexed as the R-3m space group, as indicated by the solid curve. The splitting of the (006), (012) and (018), (110) reflections suggests the formation of a highly ordered hexagonal layered structure [20]. We further performed a similar Rietveld analysis for other compounds, and software analysis results are shown in Table 1. The final refinements were satisfactory, with R_{WP} and R_I (reliable factor based on the integrated intensity) being sufficiently small. The lattice parameters of all the samples differed slightly. Figure 3 shows the regularity of (a) lattice parameters a and c and (b) lattice volume V with the change of PVA mass fraction. The lattice parameters had minimum values at x = 10.0 wt%, indicating the stability of the lattice of these samples. Compared with x = 0.0 wt%, the lattice

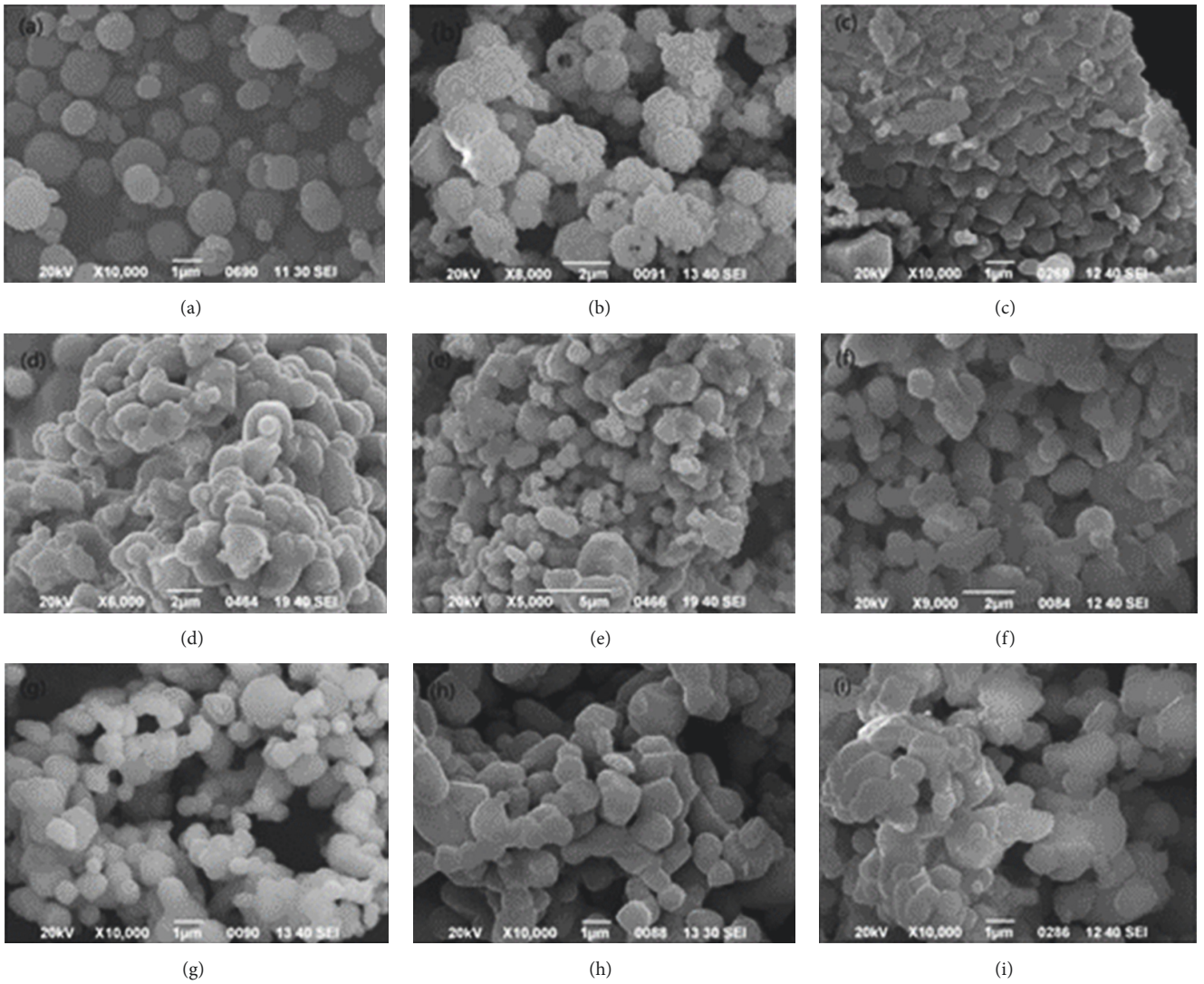

FIGURE 1: SEM images of (a) a complete spherical shell, (b) broken MnO_2 hollow microspheres, and $Li_{1.25}Ni_{0.2}Co_{0.333}Fe_{0.133}Mn_{0.333}O_2$ samples for (c) $x = 0.0$ wt%, (d) $x = 2.5$ wt%, (e) $x = 5.0$ wt%, (f) $x = 7.5$ wt%, (g) $x = 10.0$ wt%, (h) $x = 12.5$ wt%, and (i) $x = 15.0$ wt%.

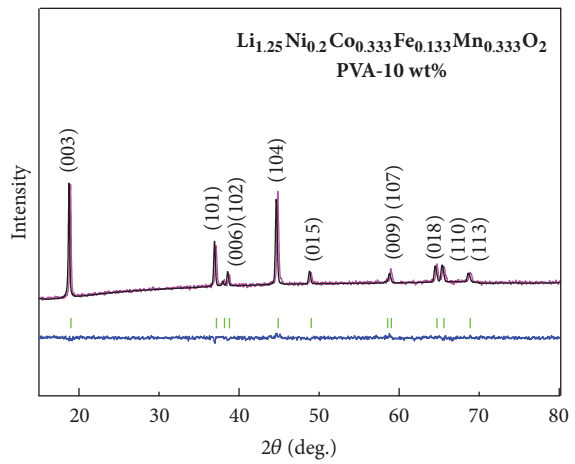

FIGURE 2: Refined XRD pattern of $Li_{1.25}Ni_{0.2}Co_{0.333}Fe_{0.133}Mn_{0.333}O_2$ ($x = 10.0$ wt%). The black crosses represent the measured points, and the pink curve is the fitted line. The green marks indicate the peak positions, and the blue line is the error curve.

Table 1: Structural parameters of $Li_{1.25}Ni_{0.2}Co_{0.333}Fe_{0.133}Mn_{0.333}O_2$ are refined by the Rietan-FP.

PVA content	a (Å)	c (Å)	V (Å^3)	R_{WP} (%)	R_I (%)	S
0.0%	2.86(1)	14.22(8)	100.9(1)	6.592	5.196	1.0932
2.5%	2.86(1)	14.25(5)	101.0(6)	6.707	5.332	1.0903
5.0%	2.86(3)	14.24(6)	101.1(7)	5.928	5.726	1.0021
7.5%	2.86(5)	14.26(9)	101.5(0)	6.528	5.160	1.0874
9.0%	2.86(1)	14.21(9)	100.8(6)	6.374	5.082	1.0570
10.0%	2.85(3)	14.18(0)	99.9(6)	6.764	5.285	1.1181
11.0%	2.85(7)	14.20(2)	100.4(6)	6.497	5.168	1.0187
12.5%	2.86(1)	14.22(2)	100.8(3)	6.615	5.784	1.2039
15.0%	2.86(3)	14.23(6)	101.0(8)	6.401	5.087	1.0514

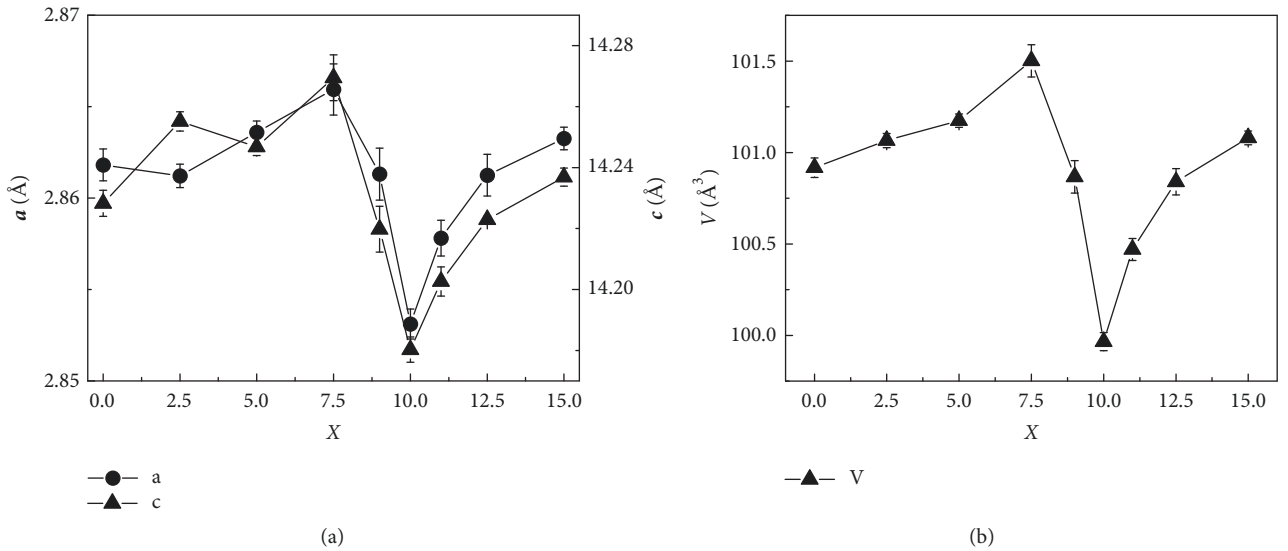

Figure 3: Variation of (a) lattice parameters a and c and (b) lattice volume V of the pristine sample and PVA-auxiliary samples, where x is the PVA content.

volume of $Li_{1.25}Ni_{0.2}Co_{0.333}Fe_{0.133}Mn_{0.333}O_2$ (x = 10.0 wt%) was reduced by 0.94%.

The electrochemical performance of the original and PVA-auxiliary lithium-rich manganese-based cathode samples was investigated at 2.5 and 4.5 V at different rates using lithium metal as the anode. The charge curves for various cycles at a rate of 0.1 C are presented in Figure 4(a). The smooth curves indicate that the electrode material had a stable structure within the tested voltage range [21]. For the pristine sample, the first discharge capacity was 141.5 mAhg^{-1} and after 50 cycles, it faded to 122 mAhg^{-1}, and the capacity loss was 16%.

For the PVA-auxiliary lithium-rich manganese-based sample (x = 10.0 wt%), the first discharge capacity was 206.0 mAhg^{-1} and after 50 cycles, it faded to 180.7 mAhg^{-1}, and the capacity loss was only 14%. It can thus be concluded that the use of a moderate PVA-auxiliary sol-gel process can enhance the specific capacity of the sample. This result occurs because the surface area is affected by the PVA content, and the increased surface area provides favorable conditions for the lithium ion insertion/extraction process. As the number of cycles increases, the discharge capacity of all samples decreases slowly, most likely due to structural deformation and/or side reactions during charge and discharge.

Figure 4(b) shows the cycle performances of all the materials under different rate. Classically, at high current rates, the specific volume drops, which may be due to an increase in electrode polarization during the cycle observed by previous researchers.

Under the various rates, specific capacities of PVA-auxiliary sample (x = 10.0 wt%) are always higher than other samples. Especially in 2 C rate, compared with PVA-auxiliary sample (x = 0.0 wt%), PVA-auxiliary sample (x = 10.0 wt%) has 2.5-fold superior rate capabilities. More importantly, when the magnification returns to 0.1 C, the capacity can be closest to the initial value. This suggests that the cathode material (x = 10.0 wt%) has an excellent reversibility. The results in Figures 4(a) and 4(b) indicate that the optimal electrochemical performance of coin cells was achieved for the PVA-auxiliary sample (x = 10.0 wt%).

To determine the rate capability of the sample, the battery was cycled between 2.5 and 4.5 V at different current rates of 0.1 C. The results are shown in Figure 5. The rate capability of the PVA-auxiliary sample is significantly higher

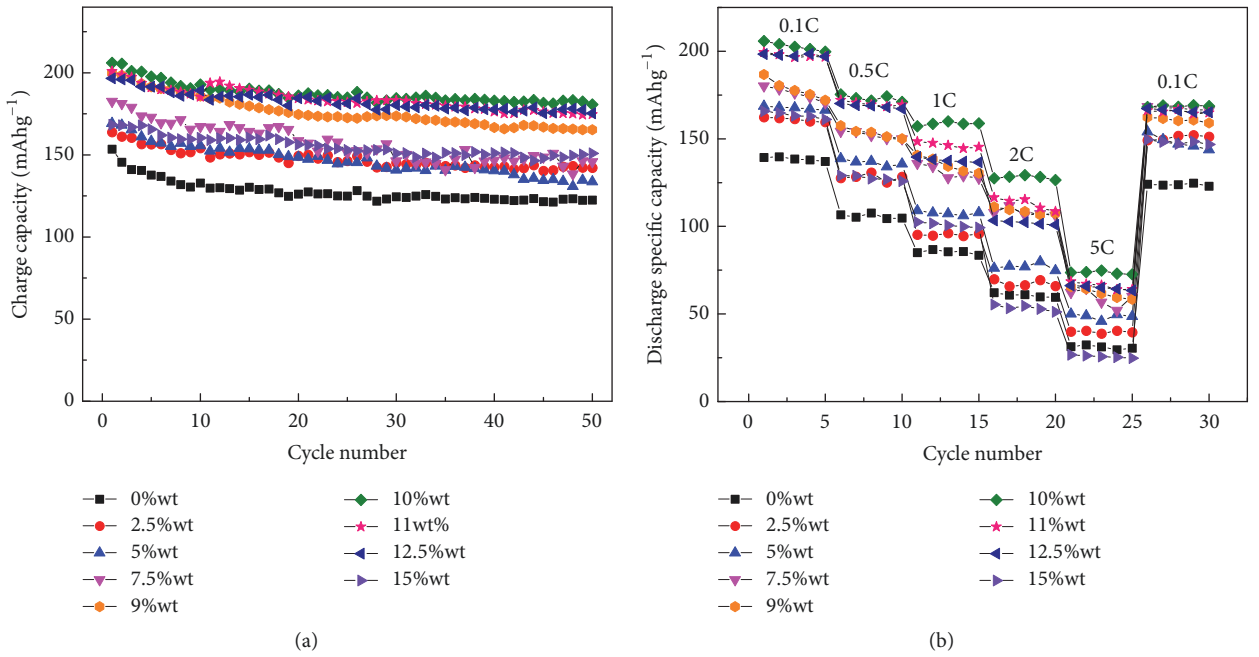

FIGURE 4: (a) Charge curves of pristine and PVA-auxiliary lithium-rich manganese-based cathode materials at 0.1 C; (b) rate capabilities of the x = 0.0–15.0 wt% cathodes.

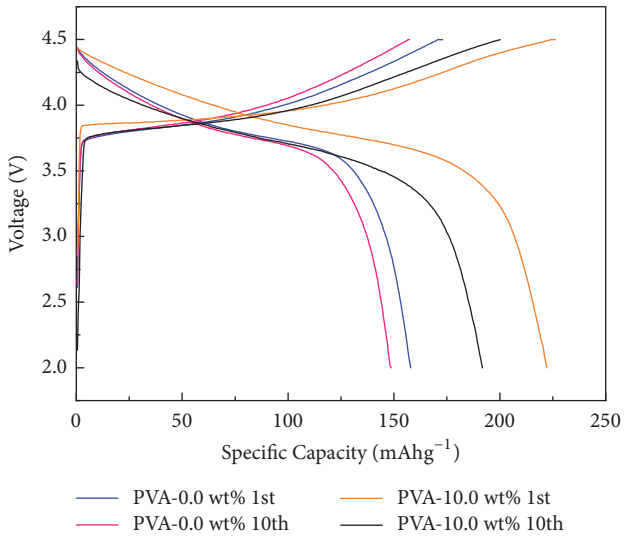

FIGURE 5: Charge/discharge curves of $Li_{1.25}Ni_{0.2}Co_{0.333}Fe_{0.133}Mn_{0.333}O_2$ (x = 0.0 and 10.0 wt%) cathodes at the rate of 0.1 C.

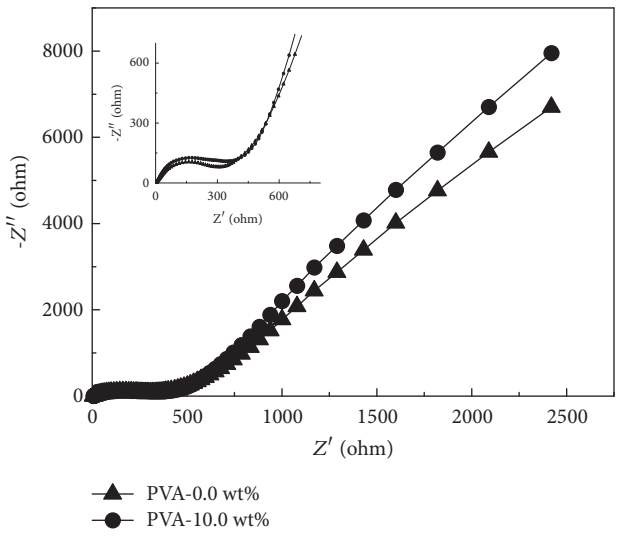

FIGURE 6: Cathodic EIS spectra of $Li_{1.25}Ni_{0.2}Co_{0.333}Fe_{0.133}Mn_{0.333}O_2$ (x = 0.0 and 10.0 wt%) materials. The inset shows the cathodic EIS spectra in the low-z' region.

than the original sample. Compared with other samples, the PVA-auxiliary sample (x = 10.0 wt%) has an excellent rate performance, because the PVA-auxiliary method reduces the charge-transfer resistance and enhances the reaction kinetics [22].

To study the reaction kinetics of the electrode materials, as shown in Figure 6, the EIS is tested with three electrode units in the frequency range of 10^{-1} to 10^5 Hz. In this region, a slanted line and semicircle were observed. The Z'-intercept between the composition of the battery and the electrolytic resistance in the high frequency region corresponds to the ohmic resistance (R_e).

The middle-frequency semicircle is associated with the charge-transfer resistance (R_{ct}) at the interface of the electrode and electrolyte [23]. The lithium ion scattering relationship in the cathode material is reflected on the oblique line of the low velocity region of the Warburg impedance (Z_w). The charge-transfer resistance of the x = 10.0 wt% sample was

300 Ω, which is smaller than that of the pristine sample (400 Ω). One possible explanation for this result is that the ion transport of the PVA-auxiliary sample is relatively faster. The reduction in charge transfer resistance clearly demonstrates the importance of electron conductivity and Li^+ diffusion when cycling at high current rates, which is closely related to rate capability and charge and discharge cycle data.

5. Conclusions

In this study, a lithium-rich manganese-based cathode material, $Li_{1.25}Ni_{0.2}Co_{0.333}Fe_{0.133}Mn_{0.333}O_2$, was synthesized using a PVA-auxiliary sol-gel process, and the effects of the PVA content on the crystal structure and morphology were investigated using XRD and SEM analyses. Compared with the pristine material, the PVA-auxiliary material (x = 10.0 wt%) after the 50 cycles of 0.1 C, the capacity holding rate is 27.7%, and the capacity at 5 C is 74.8 $mAhg^{-1}$. The improved performance of the PVA-auxiliary sample resulted from the effective reduction of the charge-transfer resistance and enhancement of the reaction kinetics. Because of the role of PVA, the rate capability and circulation of $Li_{1.25}Ni_{0.2}Co_{0.333}Fe_{0.133}Mn_{0.333}O_2$ are improved.

Data Availability

The parameters and data used to support the findings of this study are included within the article.

Conflicts of Interest

The authors declare that they have no conflicts of interest.

Acknowledgments

This work is supported by the National Natural Science Foundation of China (NSFC, 11144007) and National Natural Science Foundation of Shandong Province (ZR2016AM27).

References

[1] P. L. Taberna, S. Mitra, P. Poizot, P. Simon, and J. M. Tarascon, "High rate capabilities Fe_3O_4-based Cu nano-architectured electrodes for lithium-ion battery applications," *Nature Materials*, vol. 5, no. 7, pp. 567–573, 2006.

[2] T. Ohzuku, A. Ueda, M. Nagayama, Y. Iwakoshi, and H. Komori, "Comparative study of $LiCoO_2$, $LiNi_{12}Co_{12}O_2$ and $LiNiO_2$ for 4 volt secondary lithium cells," *Electrochimica Acta*, vol. 38, no. 9, pp. 1159–1167, 1993.

[3] Y. Gu, D. Chen, and X. Jiao, "Synthesis and electrochemical properties of nanostructured LiCoO 2 fibers as cathode materials for lithium-ion batteries," *The Journal of Physical Chemistry B*, vol. 109, no. 38, pp. 17901–17906, 2005.

[4] J. Hong, D.-H. Seo, S.-W. Kim, H. Gwon, S.-T. Oh, and K. Kang, "Structural evolution of layered Li1.2Ni0.2Mn 0.6O2 upon electrochemical cycling in a Li rechargeable battery," *Journal of Materials Chemistry*, vol. 20, no. 45, pp. 10179–10186, 2010.

[5] J. M. Tarascon, E. Wang, F. K. Shokoohi, W. R. Mckinnon, and S. Colson, "ChemInform Abstract: The Spinel Phase of LiMn2O4 as a Cathode in Secondary Lithium Cells," *ChemInform*, vol. 22, no. 49, pp. no–no, 1991.

[6] A. Yamada, S. C. Chung, and K. Hinokuma, "ChemInform Abstract: Optimized LiFePO4 for Lithium Battery Cathodes.," *ChemInform*, vol. 32, no. 29, pp. no–no, 2001.

[7] Y. M. Sun, X. L. Hu, W. Luo, and Y. H. Huang, "Self-assembled mesoporous CoO nanodisks as a long-life anode material for lithium-ion batteries," *Journal of Materials Chemistry*, vol. 22, no. 27, pp. 13826–13831, 2012.

[8] K. Zhong, X. Xia, B. Zhang, H. Li, Z. Wang, and L. Chen, "MnO powder as anode active materials for lithium ion batteries," *Journal of Power Sources*, vol. 195, no. 10, pp. 3300–3308, 2010.

[9] C. Nithya, R. Thirunakaran, A. Sivashanmugam, G. V. M. Kiruthika, and S. Gopukumar, "High-capacity sol-gel synthesis of LiNixCoyMn 1-x-yO2 ($0 \le x, y \le 0.5$) cathode material for use in lithium rechargeable batteries," *The Journal of Physical Chemistry C*, vol. 113, no. 41, pp. 17936–17944, 2009.

[10] D. Wang, X. Li, Z. Wang et al., "Role of zirconium dopant on the structure and high voltage electrochemical performances of LiNi0.5Co0.2Mn0.3O2 cathode materials for lithium ion batteries," *Electrochimica Acta*, vol. 188, pp. 48–56, 2016.

[11] Q. Chang, H. Zhang, X. Wang et al., "Structure and electrochemical performance of hollow microspheres of LiFexNi1/3-xCo1/3Mn1/3O2 ($0.000 \le x \le 0.267$) as cathodes for lithium-ion batteries," *RSC Advances*, vol. 5, no. 69, pp. 56274–56278, 2015.

[12] T. Rajh, O. I. Mićić, and A. J. Nozik, "Synthesis and characterization of surface-modified colloidal CdTe quantum dots," *The Journal of Physical Chemistry C*, vol. 97, no. 46, pp. 11999–12003, 1993.

[13] S. Huang, Z. Wen, X. Yang, Z. Gu, and X. Xu, "Improvement of the high-rate discharge properties of LiCoO2 with the Ag additives," *Journal of Power Sources*, vol. 148, no. 1-2, pp. 72–77, 2005.

[14] A. Diener, B. Nebe, F. Lüthen et al., "Control of focal adhesion dynamics by material surface characteristics," *Biomaterials*, vol. 26, no. 4, pp. 383–392, 2005.

[15] W. He, J. Qian, Y. Cao, X. Ai, and H. Yang, "Improved electrochemical performances of nanocrystalline Li[Li 0.2Mn 0.54Ni 0.13Co 0.13]O 2 cathode material for Li-ion batteries," *RSC Advances*, vol. 2, no. 8, pp. 3423–3429, 2012.

[16] T. Luo, X. Liu, X. Meng, H. Wu, S. Wang, and Z. Zhan, "In situ formation of LaNi0.6Fe0.4O3–δ–carbon nanotube hybrids as anodes for direct-methane solid oxide fuel cells," *Journal of Power Sources*, vol. 299, pp. 472–479, 2015.

[17] Y. Ruan, K. Wang, S. Song, J. Liu, and X. Han, "Improved structural stability and electrochemical performance of $Na_3V_2(PO_4)_3$ cathode material by Cr doping," *Ionics*, vol. 23, no. 5, pp. 1097–1105, 2017.

[18] N. Cimpoeşu, L. C. Trincă, G. Dascălu, S. Stanciu, S. O. Gurlui, and D. Mareci, "Electrochemical Characterization of a New Biodegradable FeMnSi Alloy Coated with Hydroxyapatite-Zirconia by PLD Technique," *Journal of Chemistry*, vol. 2016, Article ID 9520972, 9 pages, 2016.

[19] Y. Yin, S. Xin, and Y. Guo, "Nanoparticles Engineering for Lithium-Ion Batteries," *Particle & Particle Systems Characterization*, vol. 30, no. 9, pp. 737–753, 2013.

[20] W. Dong, Y. Sun, W. L. Chul et al., "Controllable and repeatable synthesis of thermally stable anatase nanocrystal-silica composites with highly ordered hexagonal mesostructures," *Journal of*

the American Chemical Society, vol. 129, no. 45, pp. 13894–13904, 2007.

[21] H. Kokubo, T. Honda, S. Imaizumi, K. Dokko, and M. Watanabe, "Effects of carbon electrode materials on performance of ionic polymer actuators having electric double-layer capacitor structure," *International Journal of Electrochemistry*, vol. 81, no. 10, pp. 849–852, 2013.

[22] Y. Shi and M. L. Falk, "Strain Localization and Percolation of Stable Structure in Amorphous Solids," *Physical Review Letters*, vol. 95, no. 9, 2005.

[23] Y. Zhu and C. Wang, "Strain accommodation and potential hysteresis of LiFePO4 cathodes during lithium ion insertion/extraction," *Journal of Power Sources*, vol. 196, no. 3, pp. 1442–1448, 2011.

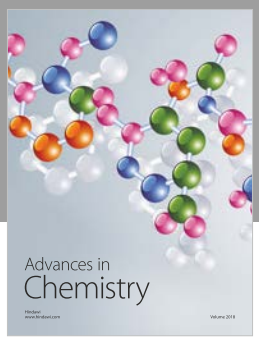

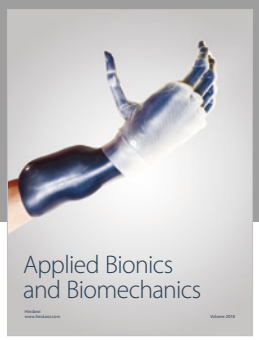

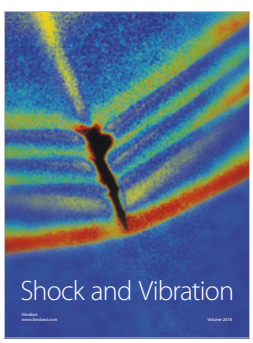

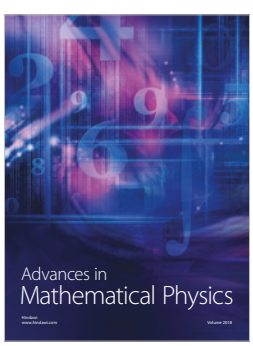

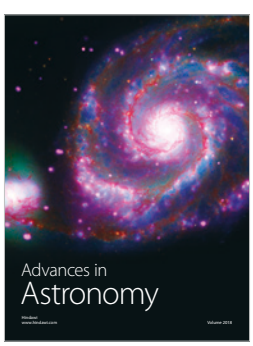

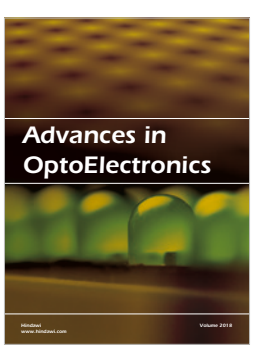

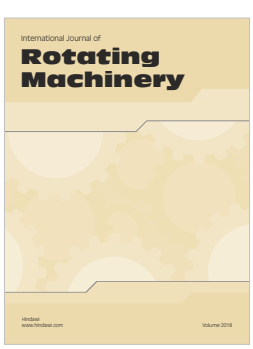

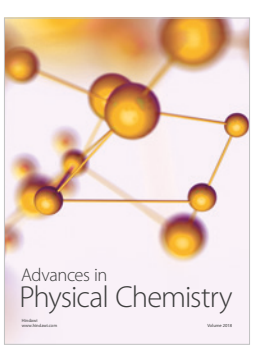

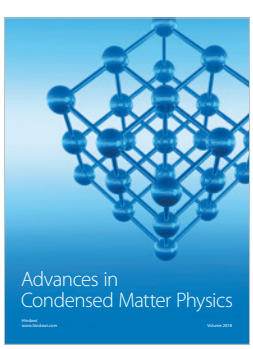

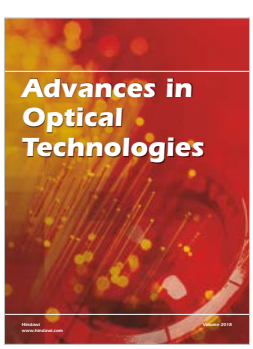

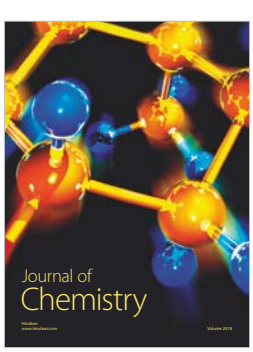

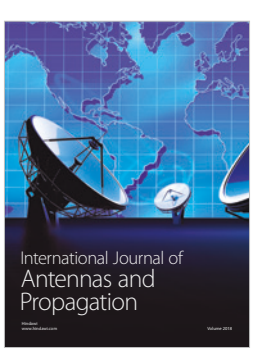

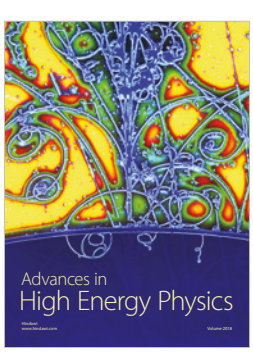

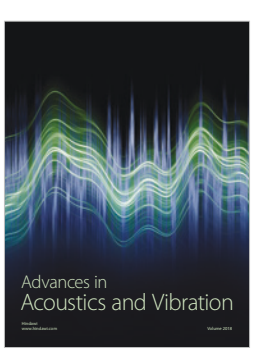

Hindawi

Submit your manuscripts at
www.hindawi.com